NUCL SCI TECH (2021) 32:100
https://doi.org/10.1007/s41365-021-00928-5

An initial study on liner-like Z-pinch loads with a novel configuration on Qiangguang-I facility

Zhan-Chang Huang[1] · Shi-Jian Meng[1] · Ze-Ping Xu[1] · Jian-Lun Yang[1] · Fu-Yuan Wu[2] · Fa-Xin Chen[1] · Xiao-Song Yan[1] · Rong-Kun Xu[1] · Zheng-Hong Li[1] · Hong-Wei Xie[1] · Yan-Yun Chu[1] · Fan Ye[1] · Jia-Min Ning[1] · Jian Lu[1] · Shu-Qing Jiang[1] · Rui-Hua Yang[1]

Received: 31 March 2021 / Revised: 26 June 2021 / Accepted: 29 June 2021 / Published online: 8 September 2021

Abstract A series of liner-like Z-pinch loads with a novel configuration have been investigated experimentally for the first time on Qiangguang-I facility in China. The metallic layer is sputtered on the inner surface of the cylindrical SiO_2 substrate tube. In the preliminary experiment, the electric current flowed through the metallic load during the prepulse. However, the currents also flowed through the outer surface of the SiO_2 substrate during the main pulse. After the dielectric length had been increased in the formal experiment, most of the current flowed through the metallic load until radial radiation peak was measured by radiation monitor. As the line mass of the metallic load increases, the peak time of radial radiation also increases. Axial ultraviolet frames indicate that the radiations are nearly azimuthally uniform at first, but the uniformity becomes worse after radial radiation peak. The clearly separated boundary between the metal plasmas and the substrate has not been observed in the experiment. Experimental results are discussed and compared with simulation using the one-dimension radiation hydrodynamics code MULTI-IFE.

Keywords Z-pinch · Liner-like · UV frame · Qiangguang-I

This work was supported by National Natural Science Foundation of China (No. 11805175).

✉ Zhan-Chang Huang
huangzhanchang@foxmail.com

1 Institute of Nuclear Physics and Chemistry, Mianyang 621900, China

2 E.T.S.I. Aeronáuticos y del Espacio, Universidad Politécnica de Madrid, 28040 Madrid, Spain

1 Introduction

There are several ways to form a Z-pinch in an experiment. In the past years, several Z-pinch configurations have been studied. For example, there are the original compression Z-pinch filled with gas, capillary discharge, the gas-embedded pinch together with micro-discharge, the wire array pinch, the gas-puff pinch, the fiber pinch, multiple shell pinch, the plasma on wire pinch, etcetera [1]. In our researches, most of the attention has been paid to studying the wire array pinches; mainly involving single wire array [2–4], nested wire array [5], conical wire array [6], cingulum array [7], and quasi-spherical wire array [8–10], for the purpose of producing an ideal x-ray source to heat inertial confinement fusion target. Professor Peng presented a novel energy technology with a local-volume-ignition fusion target to form a Z-pinch driven fusion-fission hybrid reactor in China [11]. The problems with relatively low-temperature (2–3 keV) volume ignition of DT fuel have been studied, indicating that the burning temperature will decrease as the areal density increases at the point of ignition [12]. Furthermore, simulation results revealed that forming an azimuthally uniform, and radially compact plasma shell at the moment of plasmas colliding on the foam convertor, was a key factor for the local-volume-ignition. A thin cylindrical liner with a perfect shell in the beginning seems a good choice. Liner Z-pinches have an extensive research history. Specifically, a relatively massive hollow cylinder of Al foils of 2 cm in height, 5 cm in radius and 0.25–0.75 μm thick was driven towards the axis on the Pegasus II facility and emitted soft x-rays of 125 kJ in a 200 ns pulse [13]. Similar liner implosions were also studied by Degnan et al. on the Shiva Star facility [14, 15]. When the surface material of a conductor melts, and non-uniform heating appears owing to temperature dependence in the conductivity of a material, electrothermal instabilities form immediately and act as a significant seed to subsequent MRT instability growth [16, 17]. Later, research presented a way of mitigating density perturbations arising from an electrothermal instability by using thick dielectric coatings [18]. In this paper, towards the goal of gaining a load design suitable for the local-volume-ignition fusion target, a novel configuration Z-pinch, which seems like a thin cylindrical liner surrounded by a thick dielectric substrate on the outer surface, has been studied on Qiangguang-I facility. In addition, some initial results have been analyzed. This type of novel configuration allows us to conduct liner-like experiments on relatively small-scale Z-pinch facility and get a flexible shape of the metallic load by changing the shape of the substrate tube on the future Z-pinch facilities.

2 Experimental setup

The experiments have been carried out on Qiangguang-I facility, which is able to deliver a current of 1.4–2.1 MA, with 80–100 ns rising time (10–90%) into a vacuum short-circuit load at the Northwest Institute of Nuclear Technology in China [19, 20]. The experiments comprise two stages: the preliminary experiment (called the PRE-experiment) and the formal experiment. According to the structure of electrodes and experimental experiences, the load is designed as in Fig. 1. In detail, the hollow cylindrical substrate is SiO_2. The grade of SiO_2 is JGS1, which has a transmittance of over 85% for the electromagnetic wave, with wavelengths from 200 to 800 nm [21]. The corresponding metallic layers are grown on the inner surface of SiO2 substrate via magnetron sputtering technique [22, 23]. Both 1# coating and 3# coating are sputtered with Cu. They are 200 nm ± 10% in thickness. 1# coating is utilized to make contact with the anode, and 3# coating is utilized to make contact with the cathode. 2# coating is sputtered with Al, and it acts as the imploding load. To gain a suitable thickness of 2# coating which creates a suitable imploding mass, different thicknesses of 2# coating which are listed in Table 1 are explored in these experiments. The ideal design is that the current passes through 1#, 2# and 3# coatings.

To improve the thickness uniformity and reduce the surface roughness of 2# coating, the cylindrical substrate is divided into four quarters or two halves before the magnetron sputtering process. In addition, all surfaces of the segments are polished. The surface which is sputtered as 2# coating is called 2 # surface. It is the same rule for the 1# and 3# surfaces. Figure 2 illustrates an example of polished surface characterization data from one of 2# surfaces. After

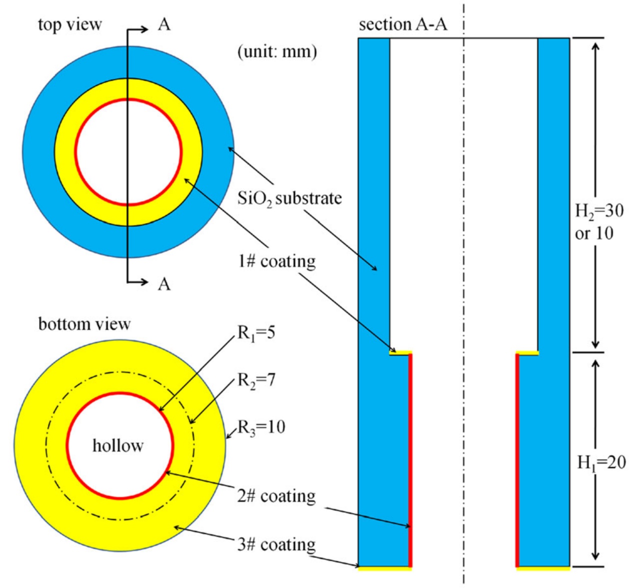

Fig. 1 (Color online) A diagram of a load. The cylindrical SiO_2 substrate, with a radius of R_3 and a height of $H_1 + H_2$, has a cylindrical hollow of R_1 in radius, and H_1 in height connecting with a cylindrical hollow of R_2 in radius and H_2 in height. The value of H_2 is 10 mm in the preliminary experiment or 30 mm in the formal experiment. The other values are the same in the preliminary and formal experiments

being polished, 1#, 2# and 3# surfaces have an RMS roughness of 1–1.3 nm. Finally, the corresponding metallic layers are sputtered on 1#, 2# and 3# surfaces. 1#, 2# and 3# coatings are continuous for the electrical conduction at the end of the magnetron sputtering process.

An experimental assembly of the load is illustrated in Fig. 3. In the PRE-experiment, to diagnose the current distribution and gain a specific experiment condition of the formal experiment, the main diagnostics include radial ultraviolet (UV) frame cameras and magnetic mini-probes. In the formal experiment, for the purpose of analysing imploding dynamics, the main diagnostics include radial radiation monitor, axial power measurement system, axial UV frame cameras, and load current monitor. The radial radiation monitor constructed with a photoelectric cell has a time response of less than 1.6 ns, and a spectral response of wavelengths from 200 to 700 nm. The axial power measurement system has a time response of less than 1.6 ns and a flat energy response from 50 to 1500 eV [24, 25]. Its measurement uncertainty is approximately 20%. The axial UV frame cameras have four frames and a spectral response of wavelengths from 262 to 272 nm. Its static spatial resolution is better than 70 μm, and its exposure time is 0.5 ns. The schematic diagram is similar to that in Ref. [26] and Ref. [27]. However, in this experiment, without using a laser, these cameras record the UV radiations which come from the load itself.

Table 1 Different thicknesses of 2# coating of different loads

Type No	Thickness (nm)	Line mass (μg/cm)	Shot No
1	235	200	18,187;18,198;18,199;18,200;18,204
2	470	400	18,188;18,192;18,193;18,194;18,195
3	705	600	18,189;18,190;18,191

The cylindrical substrates of shot18194, shot18195, shot18200, and shot18204 are assembled with two half-cylindrical segments (shown in the A-A section view in Fig. 1); the others are assembled with four quarter-cylindrical segments. The actual thickness of every load has been made to a tolerance of less than 10% of the design value. The thickness uniformity of 2# coating is better than 75% for the half segments, and 90% for the quarter segments.

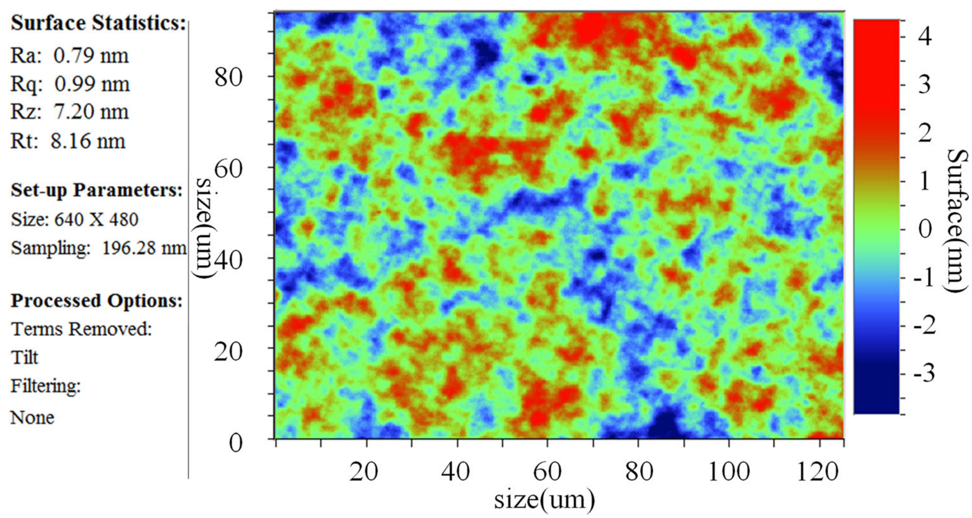

Fig. 2 (Color online) Surface map of 2# surface of a polished substrate. The value of Ra on the left is the RMS roughness

3 Results and analysis

In the PRE-experiment, the line mass was 200 μg/cm for all of the metallic loads. In addition, the current had a prepulse. The interior current of the load was measured by using two magnetic mini-probes, placed 2.5 mm away from the center of the load in a symmetrical position that is illustrated in Fig. 3a. The schematic diagram is similar to that in Ref. [5]. The total current was also measured by the Rogowski coil, which was located 22.5 cm away from the axis of the load [28]. The time zero, which is similar to that in this article, is defined by the linearly extrapolated leading edges of the main current pulse (between 10 and 90% of peak), and the results are illustrated in Fig. 4. During the prepulse of current, all of the currents flowed through the interior metallic load. The measured current in the interior of the liner is different between 1# mini-probe and 2# mini-probe for the same shot. The results in the same position of shot17273 and shot17274 are also different. The main reason is that the distribution of current during the prepulse is not azimuthally symmetrical. Later, the result of the magnetic probe was significantly less than the total current during the main pulse, indicating that some of the current was still flowing through the SiO_2 substrate.

The radial UV radiations were also measured by the radial UV frame cameras, illustrated in Fig. 5. Since there was a step of 2 mm height at the cathode, and the *H* is 20 mm in the PRE-experiment in Fig. 3a, the height of the load in the radial view was exactly 18 mm. Before the main current, the metallic load was heated by the prepulse. The UV radiations from the metallic load could be distinguished, indicating that all of the current flowed through the metallic load during the prepulse. However, the radiations were not uniform, as illustrated in Fig. 5a. During the main current pulse, as the SiO_2 was also heated, it was hard to distinguish where the radiations originated from. Since the length of the dielectric was not large enough to prevent the currents from flowing through the outer surface of the SiO_2 substrate, the SiO_2 in the outer surface was also ionized, as illustrated in Fig. 5c. To reduce these influences, the prepulse of current has been weakened as low as possible, and the H in Fig. 3a has been increased from 20 to 40 mm in the formal experiment.

3.1 Current and radial radiation

In the formal experiment, the total currents were measured by the Rogowski coil. The radial radiations with

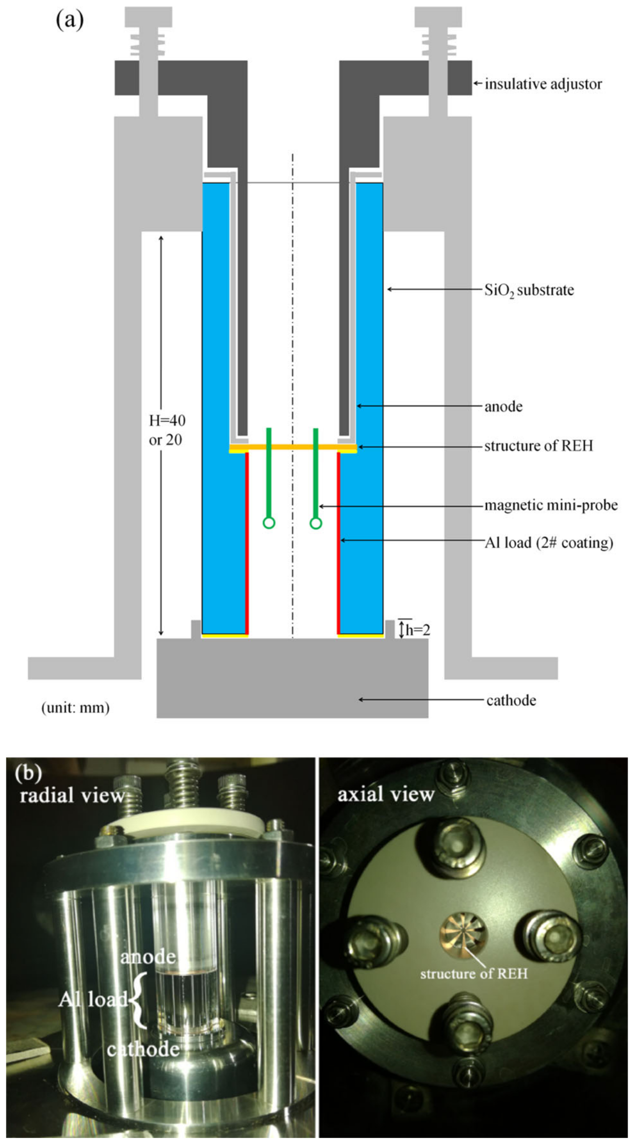

Fig. 3 (Color online) An experimental assembly: **a** a diagram; **b** a color picture. The material of the structure of REH is copper. The value of H is 20 mm in the preliminary experiment or 40 mm in the formal experiment when the vacuum chamber reached a pressure of approximately 8×10^{-3} Pa

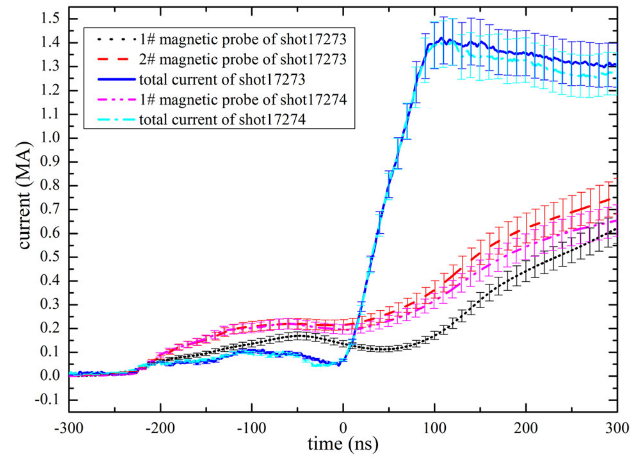

Fig. 4 (Color online) The current curves from different detectors in the PRE-experiment

wavelengths from 200 to 700 nm were recorded by the radial radiation monitor. Their results are illustrated in Fig. 6. The radial radiations increased along with the current and decreased before the current peak. The main reason is the breakdown of the SiO_2 substrate [29], which decreases the transparency of electromagnetic wave of wavelengths from 200 to 700 nm. At the start of current, the metallic load is heated by the current and then is ionized and moves inward, and the radiations (200 nm–700 nm) can be transmitted through the SiO_2 substrate. Later, the SiO_2 substrate is also heated by the metallic load plasmas until the metallic load is peeled from the substrate [18]. In addition, the SiO_2 substrate is ionized, and 2# surface is destroyed. Furthermore, the transparency of the electromagnetic wave of wavelengths from 200 to 700 nm within the surface of the ionized substrate decreases. After the metallic load is peeled from the substrate, the emission of the electromagnetic wavelengths from 200 to 700 nm coming from these plasmas cannot be transported through the destroyed 2# surface. At that time, the signal recorded by the detector is mainly from the region of the ionized substrate. Therefore, the peak time of the radiation monitor could be adopted for the indication of Al separated from SiO_2. As illustrated in Fig. 7, although the rise time of the current does not increase significantly, the peak time of the radiation slightly increases when the line mass of the metallic load increases.

The implosion process is simulated by the one-dimension MULTI program [30, 31]. This program considers all the materials as cold plasmas with 0.0258 eV at the beginning of the simulation. Therefore, the liner ablation is not considered carefully. In addition, the SiO_2 substrate has a large resistivity, enough to prevent the current from flowing through it at the start. The substrate is mainly heated by the heat exchange and radiations of plasmas. During the simulation, the experimental current and parameters of shot18187, shot18188 and shot18189 are served as the input. In addition, the simulation is carried out in one dimension, beginning from − 20 ns and considering the radiation magneto-hydrodynamic process. The implosion trajectories along with the current, are illustrated in Fig. 8. At the start of current, because the electrical resistivity of SiO_2 is significantly larger than that of Aluminum, all the current flows through the Aluminum coating. The metallic coating is converted into hot plasmas and imploded by the magnetic field. As the line mass of the metallic load increases, more time is needed for the

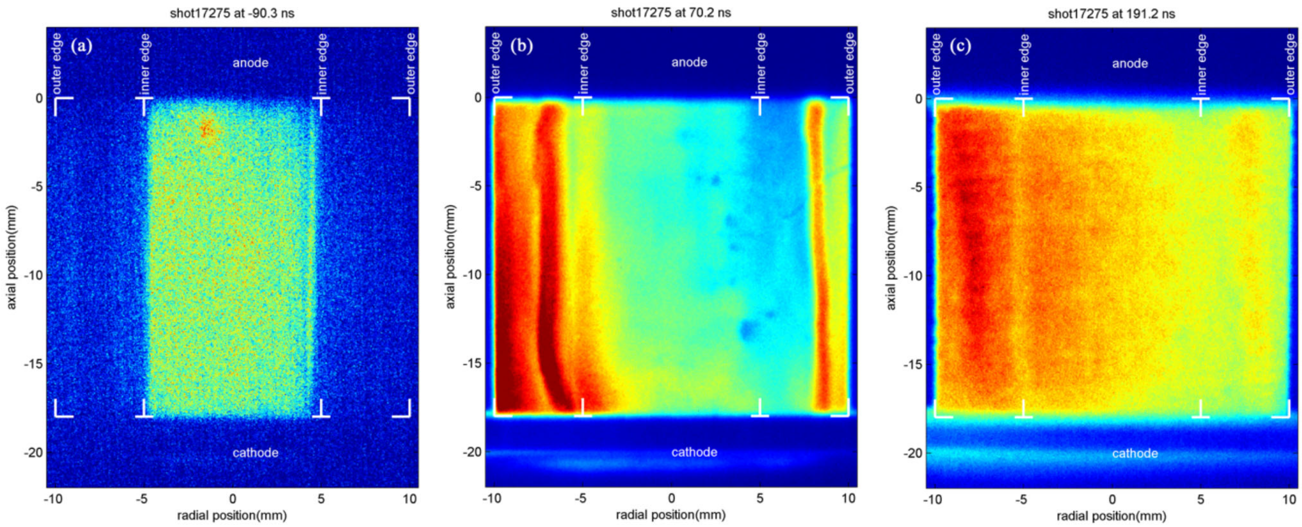

Fig. 5 (Color online) UV frame images in the PRE-experiment. The white line was the initial projective edge of SiO_2 substrate in the view of frame cameras

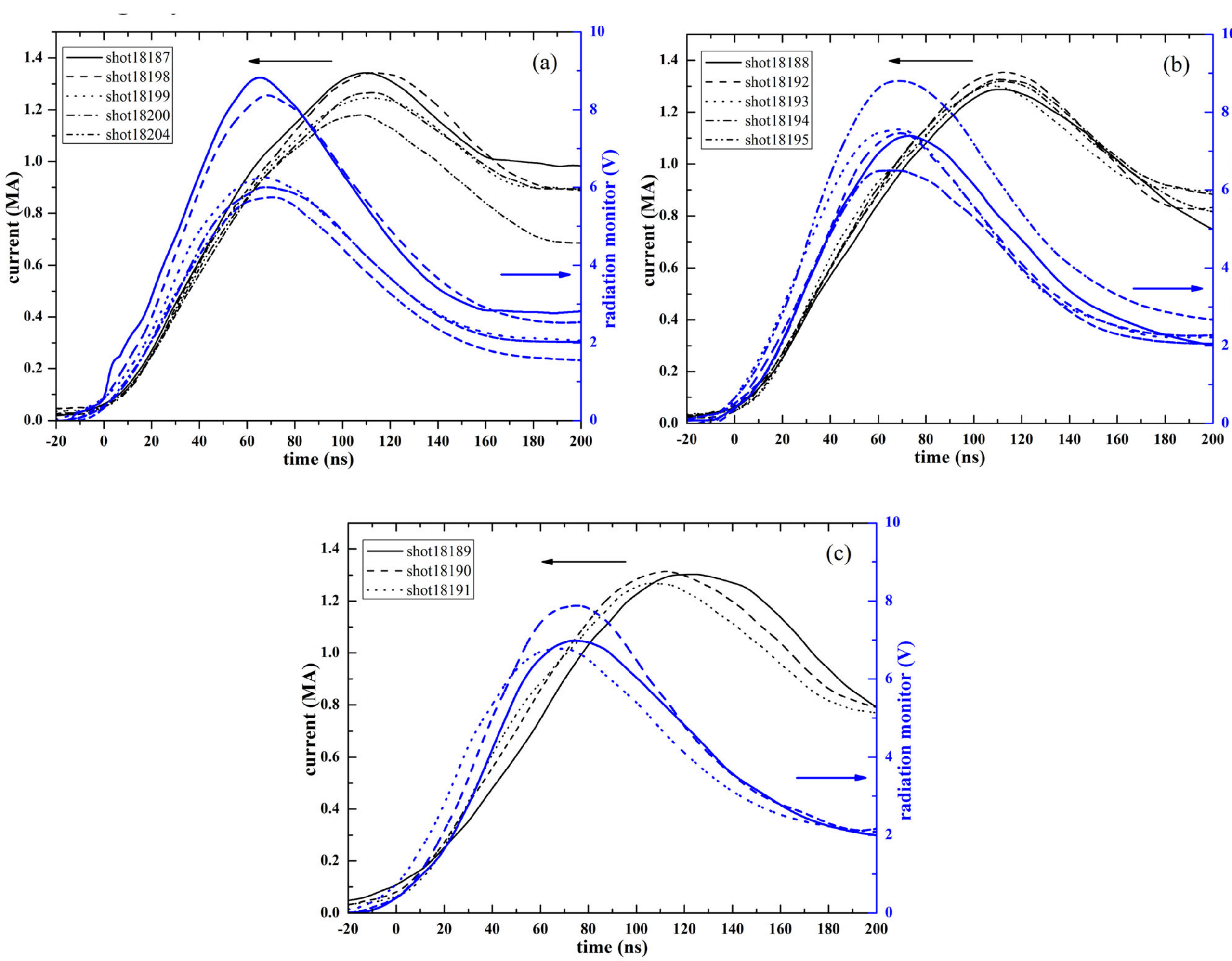

Fig. 6 (Color online) The current curves and radial radiation of different loads: **a** type 1; **b** type 2; **c** type 3

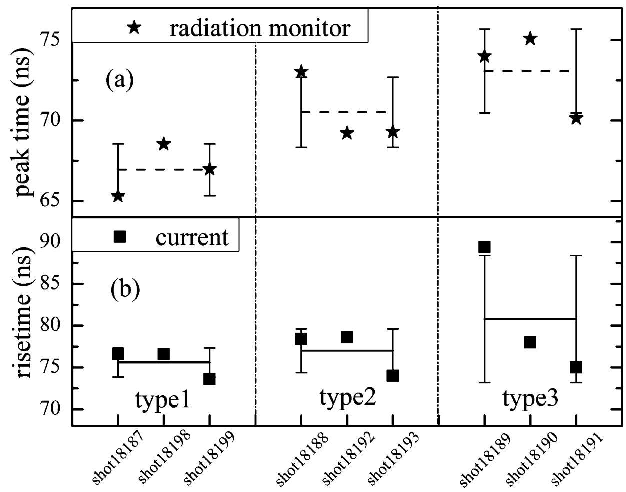

Fig. 7 The time parameters of different loads: **a** peak time of radial radiation; **b** rise time of current

metallic load to be turned into hot plasmas and separated from the SiO_2 substrate. The time increases from 67 to 70 ns, to 72.5 ns, for the experiment at an approximate 3 ns rate as shown in Fig. 7a. It increases from 28.3 ns to 34.5 ns, to 40 ns, for the simulation at an approximate 6 ns rate as shown in Fig. 8. However, the given time of Fig. 8 is earlier than that of Fig. 7a. The main reasons are that the load is considered as cold plasmas, the given time is defined as that the trajectory of Al just slightly moves 70 μm away from the trajectory of SiO_2, and the width of Al plasmas has not been taken into account carefully at this moment in the simulation. These conditions are different from the experiments.

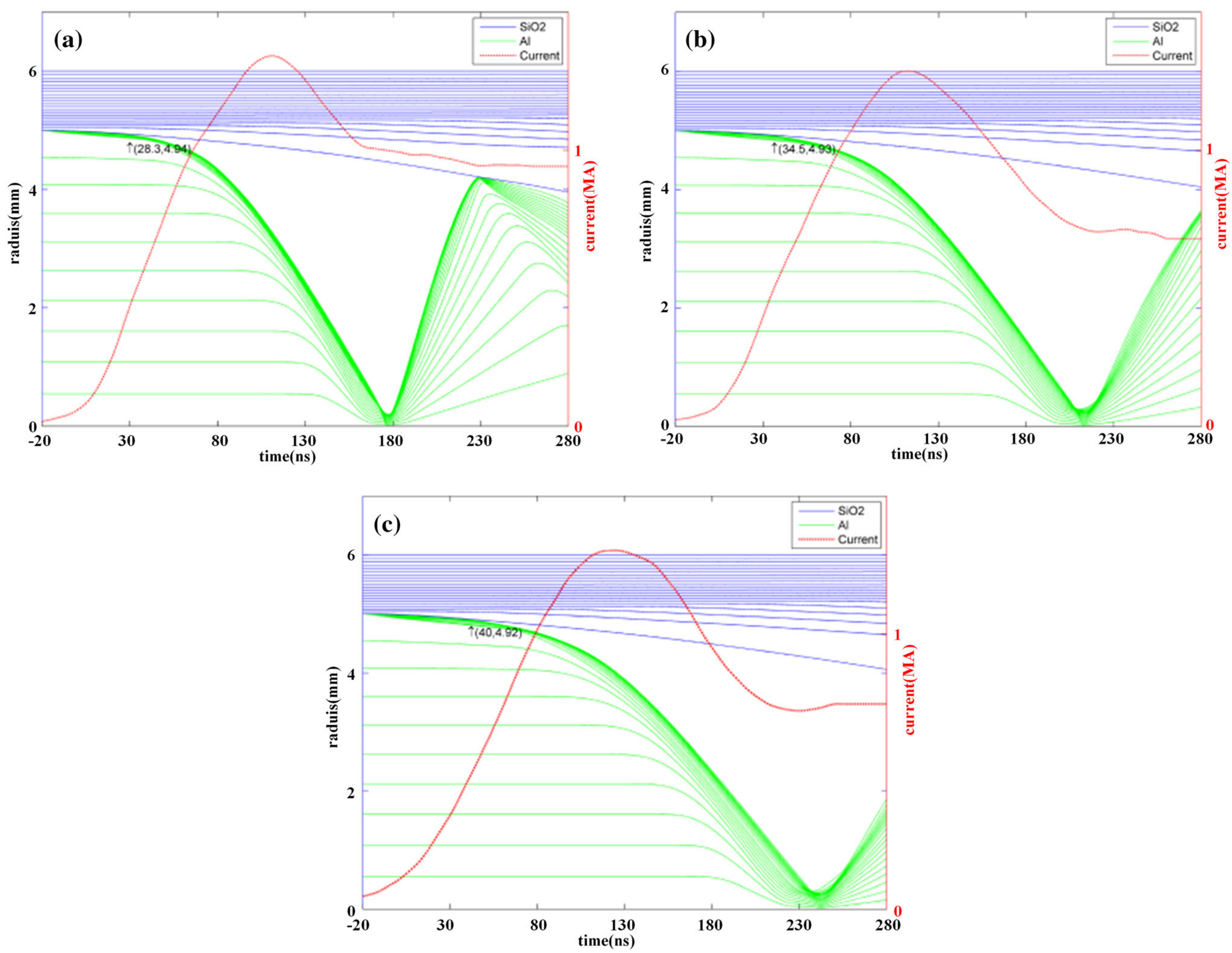

Fig. 8 (Color online) The profiles of implosion trajectories along with currents of different loads: **a** shot18187 (type 1); **b** shot18188 (type 2); **c** shot18189 (type 3). The arrows point out the time and position when the Al lightly moves 70 μm away from the SiO_2 substrate

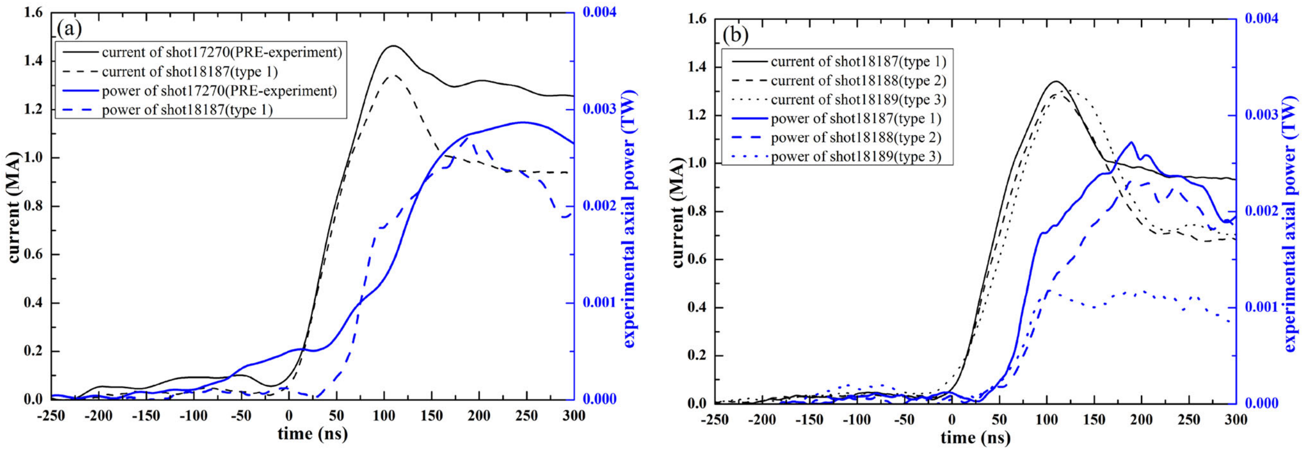

Fig. 9 (Color online) Curves of current and axial power: **a** comparison between PRE-experiment and type 1 of the formal experiment; **b** comparison among type 1, type 2 and type 3 in the formal experiment

3.2 Axial radiation property

The axial radiation power is measured by the axial power measurement system, and the result is illustrated in Fig. 9. Since there was a prepulse of current for shot17270, its axial power rose earlier and increased slower than shot18187, although they had the same line mass of the load, as it is illustrated in Fig. 9a. As the line mass of the metallic load increases, more time is spent in separating Al from the SiO_2, thus more SiO_2 is heated with more energy depositing in the substrate. Accordingly, the axial power rises consequently later and slower, and the peak decreases, as illustrated in Fig. 9b.

The frame times of the axial UV frame cameras are presented in Fig. 10 and their results are illustrated in Fig. 11. The eight dark sectors are the shadows of the opaque structure of REH illustrated in Fig. 3b. There is a hot-region in the center and some sharp jets near the assembled gaps of segments before 30 ns (indicated as 18,198–1 and 18,193–1). As illustrated in Fig. 9, when the load is heated by a prepulse of current, a negligible amount of metal is ionized, and very few precursory plasmas are formed and moved inward. These negligible axial radiations have been recorded by the axial power measurement system. The hot-region is a result of these precursory plasma radiations. The metallic layer is heated, expanded and ionized near 30–40 ns (indicated as 18,198–2 and 19,192–1). In addition, plasmas are peeled from the substrate and start to implode near 60 ns (indicated as 18,198–3 and 18,192–2). These plasmas implode inward and reach the center near 100–110 ns (indicated as 18,199–2 and 18,193–4). Its average implosion velocity is 10 cm/μs. At that time, there are still lots of plasmas being formed from the SiO_2 substrate. Later, these plasmas also take part in the implosion (indicated as 18,199–3 and

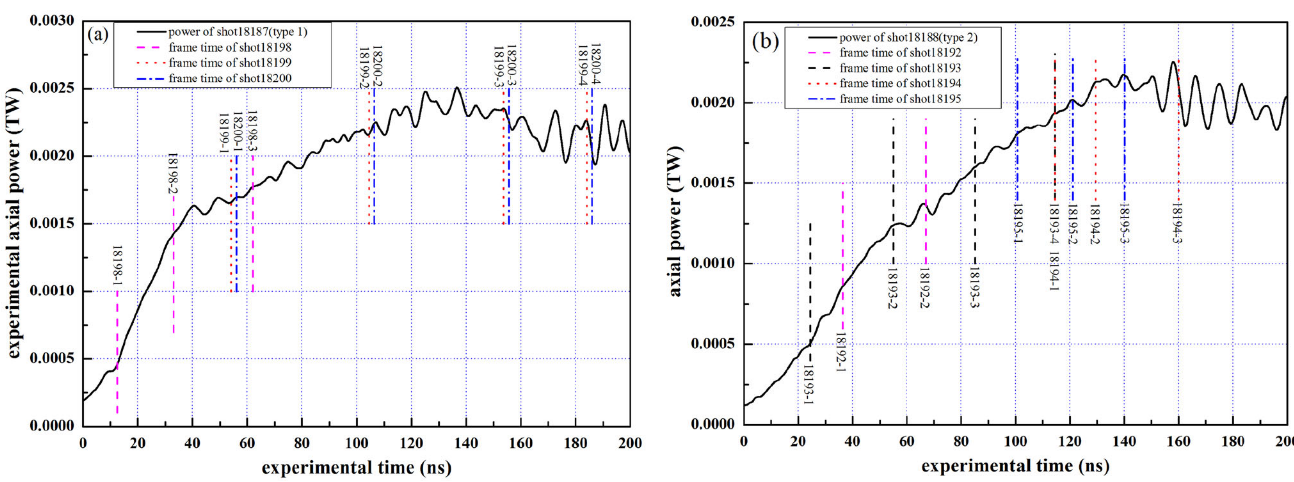

Fig. 10 The axial UV frame times of different loads

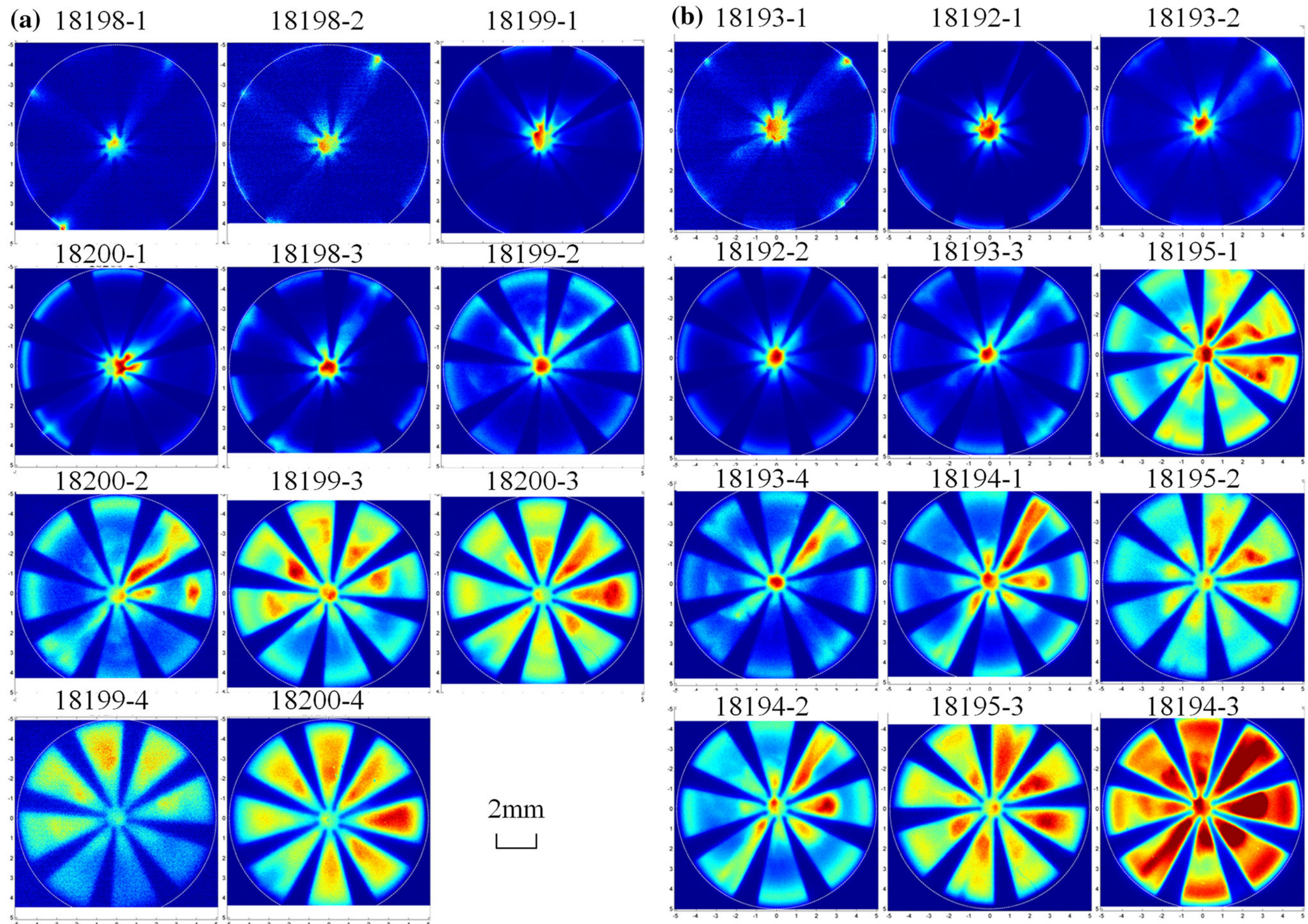

Fig. 11 (Color online) The axial UV frames of different loads: **a** type 1; **b** type 2. The white circle was the initial inner edge of SiO_2 substrate in the view of frame camera. 18,198–1 means the first frame of shot18198

18,194–2). There is no clear outer boundary of these implosion plasmas (indicated as 18,199–4 and 18,194–3).

Before 60 ns, the radiations were almost azimuthally uniform (indicated as 18,199–1 and 18,193–2). After the radial radiation peak of the radiation monitor, the plasmas are peeled from the substrate, and the radiations are not uniform anymore (indicated as 18,199–2 and 18,193–4). This asymmetry is more serious for the load assembled with two half-cylindrical substrates (indicated as 18,200–2 and 18,194–1). The uniformity of the load mass distribution in the half-cylinder is worse than that of the quarter-cylinder. One of the reasons is the asymmetry of resistivity distribution. When the temperature of the load increases, its resistivity increases rapidly. The metallic load sputtered on the substrate via the magnetron sputtering process, with loose microscopic structure, will magnify the asymmetry of resistivity. However, the current flowing through the load is not azimuthally uniform. Accordingly, it leads to worse electrothermal instability [16]. In addition, other factors, such as the early plasma ablation and the implosion, can also produce these non-uniformities at a later stage.

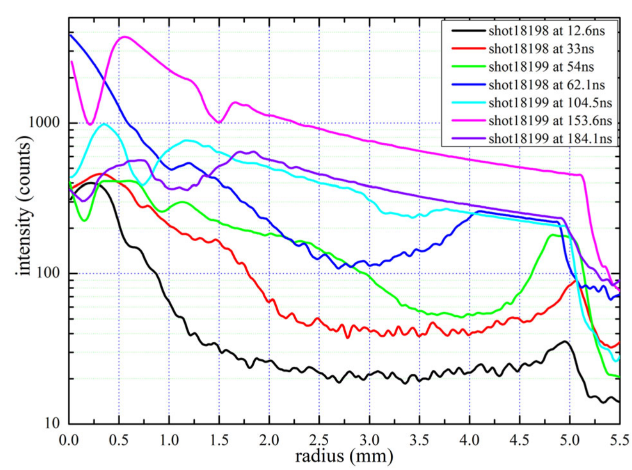

Fig. 12 (Color online) Average intensity in radial positions at different frame times

In details, one of the eight light sectors in Fig. 11a is chosen as the sample region to analyse the average intensity distribution with the radius at different frame times, illustrated in Fig. 12. Firstly, the metallic layer is heated and ionized from 12.6 ns to 33 ns near the position of the radial 5 mm. Secondly, it expanded from 0.2 mm to 0.5 mm, at the time from 33 to 54 ns. These plasmas are peeled from the substrate with a width of about 1.2 mm at 62.1 ns. There are lots of plasmas taking part in the implosion until 153.6 ns. During these times, the edge of the substrate moves outwards. At last, the implosion collapses near the center at nearly 184.1 ns.

4 Conclusion

Z-pinch loads of a novel structure have been studied at Qiangguang-I facility for the first time. Before the radial radiation peak of the radiation monitor, the metallic load can be converted into plasmas and peeled from the SiO_2 substrate because most of the currents flow through the metallic load. During the implosion, the SiO_2 substrate in contact with metal is also heated and takes part in the implosion. A novel material with a higher adiabatic factor should be chosen as the substrate, instead of SiO_2 in future experiment, to reduce this influence. In the pictures of axial UV frames, the radiations are uniform before 60 ns, but the uniformity becomes worse after the metallic plasmas are peeled from the substrate. As the mass distribution of load is not uniform enough, it leads to an asymmetry in resistivity, which seeds the electrothermal instability for this novel structure. In the next stage, we will try to improve the uniformity of mass distribution and reduce the loose microscopic structure of the metallic load, for example by adding the anneal process. The most important goal is to improve the quantity of current passing through the metal during the implosion. In addition, the simulation needs to be improved to two dimensions.

Acknowledgments We would like to thank the operating team on Qiangguang-I facility for ensuring the experimental conditions, the load fabrication team at Tongji University for their technical support, and the developers of the 1-D MULTI program.

Author contributions All authors contributed to the study conception and design. Material preparation, data collection and analysis were performed by Fa-Xin Chen, Fan Ye, Xiao-Song Yan, Fu-Yuan Wu, and Zhan-Chang Huang. The first draft of the manuscript was written by Zhan-Chang Huang and all authors commented on previous versions of the manuscript. All authors read and approved the final manuscript.

References

1. M.G. Haines, A review of the dense Z-pinch. Plasma Phys. Control. Fusion **53**, 093001 (2011). https://doi.org/10.1088/0741-3335/53/9/093001
2. Z. Wang, Z.H. Li, R.K. Xu et al., X-ray radiation power optimization in 1 MA to 4 MA wire-array implosions. Acta Phys. Sin. **60**(2), 025209 (2011). https://doi.org/10.7498/aps.60.025209
3. Z.C. Huang, J.L. Yang, R.K. Xu et al., Axially resolved radiation of tungsten wire-array Z-pinches on JULONG-I. High Energy Density Phys. **21**(1), 1–7 (2016). https://doi.org/10.1016/j.hedp.2016.09.001
4. G.X. Xia, F.Q. Zhang, Z.P. Xu et al., Radiation characteristics of single wire array Z-pinch implosion. Acta Phys. Sin. **59**(1), 97–102 (2010). https://doi.org/10.7498/aps.59.97(inChinese)
5. F. Ye, F.B. Xue, Y.Y. Chu et al., Experimental study on current division of nested wire array Z pinches. Acta Phys. Sin. **62**(17), 175203 (2013). https://doi.org/10.7498/aps.62.175203(inChinese)
6. S.Q. Jiang, F. Ye, J.L. Yang et al., Implosion characteristics of conical wire array Z pinches on " Qiangguang1" facility. Acta Phys. Sin. **61**(19), 195205 (2012). https://doi.org/10.7498/aps.61.195205
7. F. Ye, Z.H. Li, F.X. Chen et al., Investigation of ablation of thin foil aluminum ribbon array at 1.5 MA. Phys. Plasmas **23**(6), 064502 (2016). https://doi.org/10.1063/1.4952620
8. Y.Y. Chu, Z.H. Li, J.L. Yang et al., Simulation of the quasi-spherical wire-array implosion dynamics based on a multi-element model. Plasma Phys. Control. Fusion **54**(10), 105020 (2012). https://doi.org/10.1088/0741-3335/54/10/105020
9. Y. Zhang, N. Ding, Z.H. Li et al., Numerical study of quasi-spherical wire-array implosions on the Qiangguang-I facility. IEEE T. Plasma Sci. **40**(12), 3360–3366 (2012). https://doi.org/10.1109/TPS.2012.2219075
10. F.Y. Wu, Y.Y. Chu, R. Ramis et al., Numerical studies on the radiation uniformity of Z-pinch dynamic hohlraum. Matter Radiat. Extrem. **3**(5), 248 (2018). https://doi.org/10.1016/j.mre.2018.06.001
11. X.J. Peng, Z. Wang, Conceptual research on z-pinch driven fusion-fission hybrid reactor. High Power Laser Part. Beams. **26**(9), 090201 (2014). https://doi.org/10.11884/HPLPB201426.090201
12. Y.K. Zhao, B.Y. Ouyang, W. Wen et al., Critical value of volume ignition and condition of nonequilibriem burning of DT in inertial confinement fusion. Acta Phys. Sin. **64**(4), 045205 (2015). https://doi.org/10.7498/aps.64.045205(inChinese)
13. J.C. Cochrane, R.R. Bartsch, J.F. Benage et al., Direct drive foil implosion experiments on Pegasus II. AIP Conf. Proc. **299**(1), 381–387 (1994). https://doi.org/10.1063/1.2949181
14. J.H. Degnan, W.L. Baker, M.L. Alme et al., Multimegajoule electromagnetic implosion of shaped solid-density liners. Fusion Technol. **27**(2), 115–123 (1995). https://doi.org/10.1016/0920-3796(95)90112-4
15. J.H. Degnan, F.M. Lehr, J.D. Beason et al., Electromagnetic implosion of spherical liner. Phys. Rev. Lett. **74**, 98 (1995). https://doi.org/10.1103/PhysRevLett.74.98
16. K.J. Peterson, D.B. Sinars, E.P. Yu et al., Electrothermal instability growth in magnetically driven pulsed power liners. Phys. Plasmas **19**(9), 092701 (2012). https://doi.org/10.1063/1.4751868
17. K.J. Peterson, E.P. Yu, D.B. Sinars et al., Simulations of electrothermal instability growth in solid aluminum rods. Phys. Plasmas **20**(5), 056305 (2013). https://doi.org/10.1063/1.4802836
18. K.J. Peterson, T.J. Awe, E.P. Yu et al., Electrothermal instability mitigation by using thick dielectric coatings on magnetically imploded conductors. Phys. Rev. Lett. **112**(13), 135002 (2014). https://doi.org/10.1103/PhysRevLett.112.135002
19. A.C. Qiu, K. Bin, Z.Z. Zeng et al., Study on W wire array Z pinch plasma radiation at qiangguang-I facility. Acta Phys. Sin. **55**(11), 5917–5922 (2006). https://doi.org/10.7498/aps.55.5917(inChinese)
20. T. Huang, P.T. Cong, G.W. Zhang et al., Circuit simulation and analysis for Qiangguang-I Accelerator. High Power Laser and

Particle Beams **22**(4), 897–900 (2010). https://doi.org/10.3788/HPLPB20102204.0897(inChinese)
21. J.S. Du, J.H. Wu, L.L. Zhao et al., Coloration of glasses induced by space ionizing radiation. J. Inorg. Mater. **27**(4), 411–416 (2012). https://doi.org/10.3724/SP.J.1077.2012.00411
22. P.J. Kelly, R.D. Arnell, Magnetron sputtering: a review of recent developments and applications[J]. Vacuum **56**(3), 159–172 (2000). https://doi.org/10.1016/S0042-207X(99)00189-X
23. Q. Yi, Q.S. Huang, X.M. Wang et al., Structure and extreme ultraviolet performance of Si/C multilayers deposited under different working pressures. Appl. Opt. **56**(4), C145–C150 (2017). https://doi.org/10.1364/AO.56.00C145
24. Z.C. Huang, J.L. Yang, R.K. Xu et al., Design of flat response plastic scintillator. High Power Laser and Part. Beams. **28**(11), 28112001 (2016). https://doi.org/10.11884/HPLPB201628.160133
25. Q.Y. Hu, J.M. Ning, F. Ye et al., Applications of thin film plastic scintillator in measurement of soft x rays generated from Z-pinch implosion. Rev. Sc. Instrum. **89**(10), 103112 (2018). https://doi.org/10.1063/1.5049449
26. F.X. Chen, J.H. Feng, L.B. Li et al., Study of Z-pinch dynamic hohlraum shadowgraphy. Acta Phys. Sin. **62**(4), 45204–045204 (2013). https://doi.org/10.7498/aps.62.045204
27. H.W. Xie, F.X. Chen, Q. Yi et al., Application of ultraviolet laser probe in Z-pinch. High Power Laser and Part. Beams. **29**(04), 29042001 (2017). https://doi.org/10.11884/HPLPB201729.160506
28. N. Guo, L.P. Wang, J.J. Han et al., Differential loop for measuring 1 MA/100 ns pulsed high current. High Power Laser and Part. Beams **24**(3), 519–523 (2012). https://doi.org/10.3788/HPLPB20122403.0519
29. C. Li, X. Li, K.H. Zhang et al., Femtosecond laser induced breakdown in fused silica by linearly, circularly and elliptically polarized lasers. Acta Photonica Sinica. **43**(1), 0132002 (2014). https://doi.org/10.3788/gzxb201443s1.0132002
30. R. Rafael, R. Schmalz, J. Meyer-ter-Vehn, MULTI—A computer code for one-dimensional multigroup radiation hydrodynamics. Comput. Phys. Commun. **49**(3), 475–505 (1988). https://doi.org/10.1016/0010-4655(88)90008-2
31. F.Y. Wu, R. Ramis, Z.H. Li et al., Numerical Simulation of the Interaction Between Z-Pinch Plasma and Foam Converter Using Code MULTI (#8353). Fusion Sci. Technol. **72**(4), 726–730 (2017). https://doi.org/10.1080/15361055.2017.1347458